17th Mediterranean Conference on Control & Automation
Makedonia Palace, Thessaloniki, Greece
June 24 - 26, 2009

Experimental Tissue Parameter Identification for Use in Endoscopic Urological Haptic Simulators

Athanasios Dimopoulos, Evangelos Papadopoulos
Department of Mechanical Engineering
National Technical University of Athens
15780 Athens, Greece
dimotha@gmail.com, egpapado@central.ntua.gr

Karl Iagnemma
Department of Mechanical Engineering
Massachusetts Institute of Technology
Cambridge, MA 02139, USA
kdi@mit.edu

Abstract—**A method is developed for obtaining parameters for tube-like soft-tissues, to be used in urological haptic simulators. A device was designed and built that allows the acquisition of forces and displacements during endoscope insertion in a tube-like soft tissue. The device consists of a mechatronic ball screw mechanism, with a 6 DOF force/ torque sensor attached to it. The steel shaft representing the endoscope, is commanded to follow desired trajectories with micrometric accuracy under the application of an IPD controller, implemented on a dSpace 1103 system. The experimental data acquired is fitted to polynomials to yield a tissue model that can be used to predict insertion forces required for haptic simulator feedback.**

***Index Terms*: Soft tissue modeling, endoscopic surgery simulation, tissue identification, haptic feedback.**

I. Introduction

This work responds to the need for obtaining tissue force models that correspond to endoscopic surgeries, such as the one that involves the male urethra. Besides a good mechanical design of the haptic interface and a responsive real-time system, accurate tissue modeling is required in surgical simulators to achieve the best transfer of the real surgery conditions to the trainee through the haptic interface [1]. To this end, both the structure of the model and the associated parameters must be determined. Although a number of tissue modeling methods exist in the literature, to the best of our knowledge, no methods predicting insertion forces in tube-like tissues are available.

The main tissue model methods available today focus on model determination using ultrasound or Instron devices. Other models are determined through custom devices like the VESPI, [2], where liver tissue was measured in vitro. Using the ROSA-2, bovine liver in vitro, and porcine liver and spleen in vivo, were tested, [3]. The TeMPest was used to compare results to those of ROSA-2, [3]. A large number of results was acquired in a series of experiments done with the MEG, [4]. The MEG was used to test liver, spleen, stomach, small and large intestine, and even the lung in vivo. Similar work was performed for use in haptic interfaces and simulators, such as in the needle and soft-tissue interaction during needle insertion, [5, 6]. These works focus on finding a model that best describes soft tissue behavior under various loading conditions.

At the level of stress strain relationships, a number of models have been proposed. Well known material models include Maxwell's serial spring-damper model, and Voigt's parallel spring damper model. A synthesis of these two was proposed by Kelvin. A widely used, general stress strain relationship, is the exponential function of Fung, which is based on the quasi-linear viscoelasticity (QLV) theory [6]. Another stress-strain relationship is the non-linear pseudo elastic two-parameter Blatz model, [7]. This model was used for ex-vivo porcine kidney testing. Most of the models are general descriptions of tissue behavior. When it comes to soft tissues, the modeling accuracy is reduced. This is due primarily to the nonlinear behavior of soft tissues. The stress developed is correlated not only to the strain magnitude, but also to the strain rate of change. Increased anisotropy, along with hysteresis, further decrease model accuracy.

This work focuses on developing a methodology for measuring the development of stress – strain forces during endoscopic conditions in tube-like soft tissues, like the male urethra, the arteries or the intestines. A device was designed and built that simulates the insertion of the endoscope in a tube shaped soft tissue. The device mainly consists of a ball screw mechanism with a 6 DOF force/ torque sensor attached to it. The steel shaft representing the endoscope moves according to the desired trajectory inside the material representing the soft tissue. The motion is executed with micrometric accuracy under an IPD controller, and implemented on a dSpace 1103 Rapid Control Prototyping System. During the experiment, the developing endoscopic forces are recorded, along with the position of the endoscope. The experimental data acquired are fitted to polynomials and their coefficients are determined. The obtained model is simple enough to be used in real-time training haptic simulators.

II. Simulator Needs

Soft tissue surgery requires very gentle execution of surgical moves. Before proceeding with the operation, young surgeons must already have acquired some experience. Modern Virtual Surgical Simulators (V.S.S.) are very effective in training novice surgeons for a number of

reasons. (a) Training in near realistic surgical conditions is of key importance to effective training. Fortunately, modern technology has achieved a good level of realistic experience during training. (b) A virtual surgical simulator is cost effective, as the initial cost is reduced greatly with the number of trainees. (c) With a V.S.S., a novice surgeon can be trained effectively and evaluated for his/ her performance with error notification and improvement suggestions. (d) With a V.S.S., most surgical conditions can be simulated realistically and no real patient is required. The trainee gains the basic experience fast and accurately, before reaching the operating room.

Surgical simulators consist mainly of three subsystems:

- The force feedback haptic mechanism
  Through this subsystem, the user moves the endoscope in the virtual environment and receives haptic feedback (force/ torque), that corresponds to his actions.
- The visualization subsystem
  This subsystem creates the 3D environment of the virtual inner organs and tissues, and computes the deformations and reaction forces/ torques due to tissue-endoscope interactions.
- The control subsystem
  This subsystem handles the force application to the user and the data exchange between the haptic mechanism and the visualization subsystem.

To obtain a realistic experience, the haptic device must exhibit small mass and inertia, negligible friction, and high stiffness. It must also include the appropriate available degrees of freedom, gravity compensation, and overall robustness. Assuming that these conditions have been met, an accurate model describing tissue behavior is essential to a realistic trainee experience.

Here we focus on simulators for endoscopic surgeries involving the male urethra. Urethra tissues are soft and tube-shaped, and exhibit a non-linear behavior. To obtain a model of their behavior, a special device able to measure the forces developed during endoscopic surgery, is needed. The forces, along with endoscope displacement and velocity, are measured and processed to result in a suitable tissue behavior model. In the next section, the design of such a device is presented.

III. Experimental Device Design & Control

The main idea was to design a compact and robust device that could measure forces developed during endoscope insertion. To achieve this goal, we first had to choose the way the endoscopic conditions would be achieved. Among alternative ways, we chose the case of linear insertion of a steel shaft in a tube-shaped material with properties close to urethra tissue. An advantage of this setup is that linear displacement is easier to implement and the obtained data more reliable. The device should be able to hold the flexible tube fixed and to accept different kinds of tube materials, including real tissues. The steel shaft surface properties are identical to those of the real endoscope used in surgeries.

After the qualitative goals of the design have been set, device specifications were set. To simulate the forces developed in real endoscopic surgery conditions, first a geometric similarity was sought. Therefore, a steel shaft of 15 cm length (useful length) and of 1 cm diameter was specified. The steel shaft should be able to move all of its useful length inside the flexible tube, at speeds close to 2 mm/s. The flexible tube employed was specified to have nearly the same dimensions to those of the male urethra tissue, and with comparable properties. For obtaining a more general model of tissue behavior, speeds of up to 40 mm/s were specified. For an accurate model development, accurate data was in need. The desired position measurement resolution was set to 0.1 mm, and zero backlash conditions for the moving parts were required.

To achieve the above specifications, an accurate displacement measurement system was required. To measure the insertion forces, expected not to exceed 4.5 N, [1] an appropriate sensor was required.

After the coarse design goals have been set, alternative designs were explored. These were constrained by (a) the difficulty in constructing the device, (b) the availability of parts in the market, (c) whether the parts would fit and work together, and (d) the overall cost.

For the endoscope linear displacement, we chose a ball screw system with a bed and a 2 mm lead. The bed is able to move for 151 mm, in agreement to our design goals. Two linear guides with linear bearings support the bed. A 20W, DC brushed Maxon motor is used to move the ball screw system. This motor was equipped with a 500 count per revolution encoder, resulting in a 4μm per revolution resolution along the linear displacement axis. Between the bed and the steel shaft, an ATI nano17 Force/ Torque 6 DOF sensor was attached. This sensor is capable of measuring forces and torques in the endoscopic order of magnitude.

To ensure a proper design, a CAD design of the whole device was first developed, see Fig.1. Most of the parts used were off-the-shelf components, while a few others, like the bed or some supports, were constructed on a CNC machine.

A position controller, implemented on the DS1103 dSpace Rapid Control Prototyping System, was used to control the endoscope displacement.

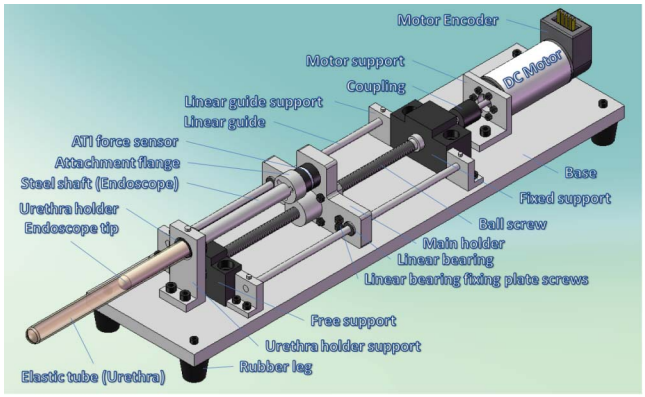

Fig. 1. The experimental identification device in SolidWorks.

To this end and to achieve the required resolution, first a model that would describe the system behavior was needed. The system equations were developed using the Bond Graph methodology, [9], see Fig. 2,

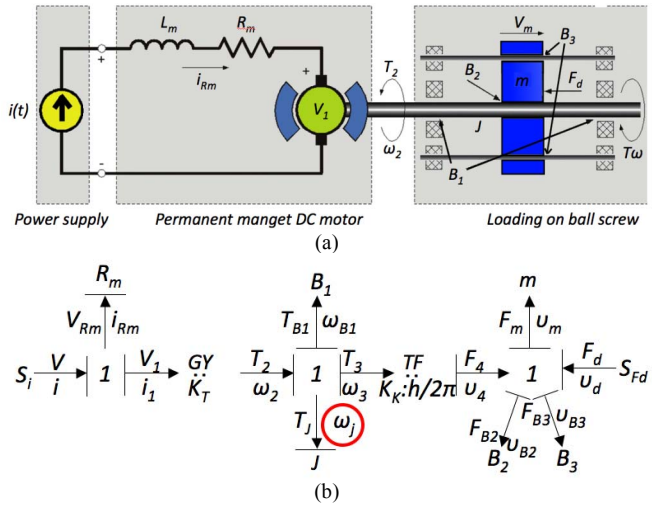

Fig. 2. Device (a) physical model and (b) the corresponding bond graph.

For the two inputs shown in Fig. 2 and neglecting nonlinear Coulomb friction, the Bond Graph methodology yields the following transfer function:

$$G_p = \left[\frac{K_T / J_{eff}}{s \cdot \left(s + B_{eff} / J_{eff}\right)}, \quad \frac{h/2 \cdot \pi}{s \cdot \left(s + B_{eff} / J_{eff}\right)} \right] \tag{3}$$

where K_T is the motor torque constant, J_{eff} is the effective moving mass inertia, B_{eff} is the effective damping coefficient, and h is the screw pitch. System parameters such as friction, damping, and inertia, are obtained next.

Static (Coulomb) friction was measured along the ball screw by the current i_c needed just to start a motion. The obtained values were fitted by two polynomials, one for the forward and one for the reverse motion, to yield:

$$i_{c,f}(x) = -0.001344 \cdot x + 0.5206 \quad [A] \tag{4}$$

$$i_{c,r}(x) = -0.0007268 \cdot x + 0.4125 \quad [A] \tag{5}$$

where x is the bed displacement in mm. With another series of constant speed experiments, the coefficient of damping was determined, according to:

$$B = \frac{K_T \cdot \left(i - i_c\right)}{\omega} \tag{6}$$

where ω is the motor angular speed.

To compute B as a function of velocity and displacement, experiments were conducted for velocities of 10 mm/s, 15 mm/s and 20 mm/s. Fig. 3 shows these forces as a function of forward displacement for a bed speed equal to 15 mm/s. The oscillation in force observed was due to small ball screw axis eccentricity, which in turn was due to a small base sqewness.

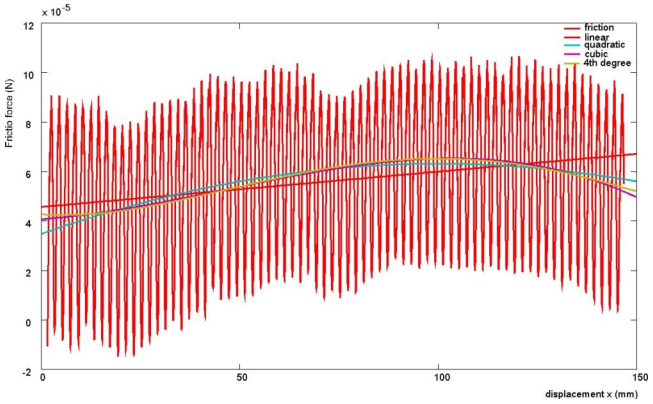

Fig. 3. Friction force vs. displacement at 15 mm/s.

For each of the three speeds, a polynomial is fitted to the data, to yield the coefficient as a function of x:

$$B_{10}(x) = -7.47 \cdot 10^{-11} \cdot x^3 + 1.09 \cdot 10^{-8} \cdot x^2 + 7.97 \cdot 10^{-8} \cdot x + 2.51 \cdot 10^{-5} \quad Nm \cdot s \cdot rad^{-1} \tag{7}$$

$$B_{15}(x) = -3.30 \cdot 10^{-11} \cdot x^3 + 4.56 \cdot 10^{-9} \cdot x^2 + 1.18 \cdot 10^{-7} \cdot x + 4.07 \cdot 10^{-5} \quad Nm \cdot s \cdot rad^{-1} \tag{8}$$

$$B_{20}(x) = -3.82 \cdot 10^{-13} \cdot x^3 - 3.2 \cdot 10^{-9} \cdot x^2 + 6.49 \cdot 10^{-7} \cdot x + 4.01 \cdot 10^{-5} \quad Nm \cdot s \cdot rad^{-1} \tag{9}$$

The above results were averaged over speed, to yield a coefficient as a function of bed displacement x:

$$B(x) = -3.60 \cdot 10^{-11} \cdot x^3 + 4.07 \cdot 10^{-9} \cdot x^2 + 2.83 \cdot 10^{-7} \cdot x + 3.53 \cdot 10^{-5} \quad Nm \cdot s \cdot rad^{-1} \tag{10}$$

Finally, to obtain a single value for B_{eff}, (10) was averaged over x to yield:

$$B_{eff} = \frac{\int_0^{150} B(x)}{150} = 5.66 \cdot 10^{-5} \quad Nm \cdot s \cdot rad^{-1} \tag{11}$$

Next, the effective inertia of the moving masses as seen from the motor side, J_{eff}, was identified. To this end, the following system of equations is used:

$$\underbrace{\begin{bmatrix} \dot{\omega}_1 & \omega_1 \\ \dot{\omega}_2 & \omega_2 \\ \dot{\omega}_3 & \omega_3 \\ \vdots & \vdots \\ \dot{\omega}_n & \omega_n \end{bmatrix}}_{\mathbf{A}} \cdot \underbrace{\begin{bmatrix} \frac{J_{eff}}{K_T} \\ \frac{B_{eff}}{K_T} \end{bmatrix}}_{\mathbf{x}} = \underbrace{\begin{bmatrix} i_1 - i_{c1} \\ i_2 - i_{c2} \\ i_3 - i_{c3} \\ \vdots \\ i_n - i_{cn} \end{bmatrix}}_{\mathbf{b}} \tag{12}$$

where $\dot{\omega}$ is the angular acceleration, and i is the motor current measured during the experiment. The motor torque constant K_T was found experimentally to be equal to 24.49 mNm/A, in accordance to motor specifications. The elements of **A** and **b** were measured during bed displacement using the motor encoder, and read by the dSpace 1103 Rapid

Control Prototyping System. The measurements were obtained with the bed moving for its total travel. The trajectory was chosen to be:

$$x(t) = 75 + 45 \cdot \sin t \quad [mm] \tag{13}$$

Solving (12) with least squares, the J_{eff} and the B_{eff} were computed as:

$$\begin{bmatrix} J_{eff} \\ B_{eff} \end{bmatrix} = \begin{bmatrix} 5.06 \cdot 10^{-6} & kg \cdot m^2 \\ 2.93 \cdot 10^{-5} & Nm \cdot s \cdot rad^{-1} \end{bmatrix} \tag{14}$$

This effective inertia value was used in control design. The value for B_{eff} in (14) differs from that in (11). Since the latter was determined directly, it was used as the nominal value.

The obtained system model and parameters were used to design a controller that could move the bed and endoscope assembly with precision. To this end, an IPD controller was employed, [8]. This controller feeds back the position error and the actual speed and has some advantages over classical PID controllers. Indeed, the IPD adds no zeros to the closed-loop transfer function, and hence the controller can be designed to exhibit zero overshoot. Pole placement was used to determine the IPD gains, so that the system would be stable, with no overshoot and negligible steady state error.

The controller was implemented on the dSpace DS1103 card. The position error achieved was typically down to ± 5 μm, as shown in Fig. 4 for a trajectory x(t) = 75+60sint. This error was bounded by 5 μm throughout the bed displacement (150mm).

Fig. 4. Mean bed position error at 5 μm.

IV. Experiments

The device built is shown in Fig. 5, along with the controller card and the motor servo amplifier. Since no biological tissue was available at the time when the device was completed, it was decided to choose a similar material allowing us to set up the appropriate methodology for obtaining the material properties.

The material had to be elastic and exhibit minimal plastic deformations. Latex was a good candidate for these requirements. The elasticity of latex, along with its tribological surface characteristics is close enough to the human urethra tissue. In addition, it deforms radially to a larger diameter endoscope, as it happens with the real tissue. The length of the latex tube was chosen 2-3 cm longer than the shaft length.

In real surgical conditions, water is used as a lubricant assisting in endoscope insertion. In this case however, water over the latex tube resulted in increased friction. Therefore, an appropriate lubricant had to be chosen. Various lubricants were tested and the best results were obtained with hydraulic fluid, i.e. very low friction between the latex tube surface and the steel shaft of the endoscope.

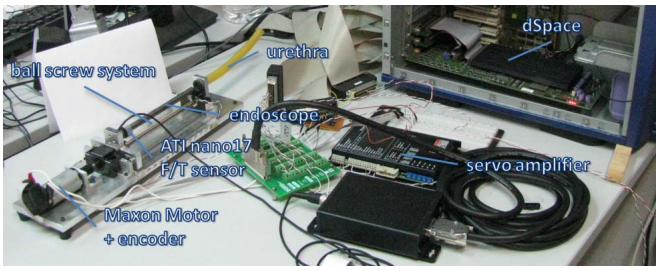

Fig. 5. The experimental device, the servo amplifier and the dSpace card.

Another important factor in preparing the experiments was the design of the insertion trajectories. The general form of these trajectories is shown in Fig. 6. Since we wanted mostly constant speed segments, the insertion trajectory was designed such that the endoscope accelerates briefly, then it moves at constant speed, then it decelerates and stops. After staying still for some time, the retraction phase starts, in which the insertion trajectory is played backwards, i.e. the endoscope accelerates backwards, then it moves with a backwards speed and finally it stops.

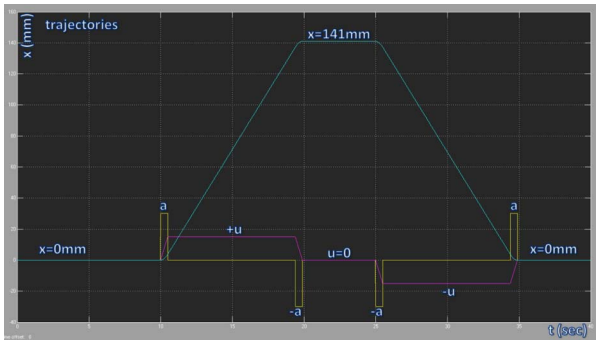

Fig. 6. The endoscope trajectory during tube insertion and retraction.

To construct the material force model, the forces developed as a function of the endoscope displacement and speed had to be determined. The developed forces were measured for endoscope speeds of 3.75 mm/s, 7.5 mm/s, 15 mm/s, 20 mm/s and 30 mm/s. During each speed experiment, endoscope force, position and velocity, motor current, and position error were measured. The forces developed on the endoscope and the endoscope position in the latex tube over time, for the above speeds, are shown in Figs. 7, 8, 9, 10, and 11.

These figures show that there is an almost linear increase of the force as a function of the endoscope displacement and a drop in its magnitude, when the

endoscope reaches the maximum insertion depth and stops. This discontinuity occurs during all acceleration or deceleration phases of the endoscope and is due to the sudden nonlinear deformation of the latex.

The force results were sampled at 1Khz. We observe that the force varies between 3 to 4 N. According to [1], the maximum forces expected during a real endoscopic surgery are about 4.5 N. Therefore, the latex tube experiments are yielding forces in the same range as the real operation and hence, this material reproduces the endoscopic conditions close enough.

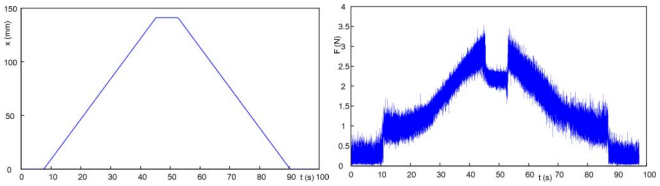

Fig. 7. Endoscope position and friction forces at 3.75 mm/s.

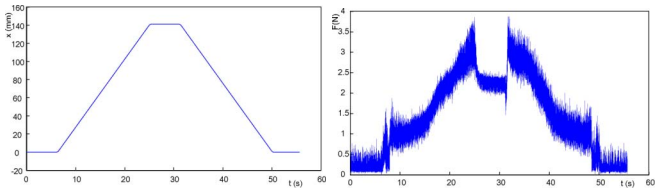

Fig. 8. Endoscope position and friction forces at 7.5 mm/s.

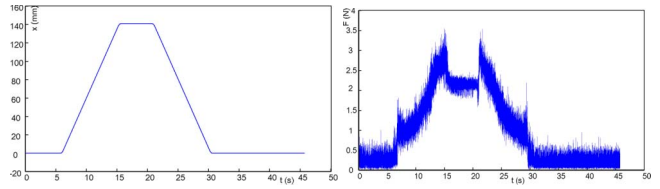

Fig. 9. Endoscope position and friction forces at 15 mm/s.

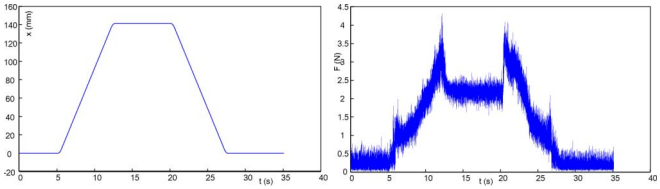

Fig. 10. Endoscope position and friction forces at 20 mm/s.

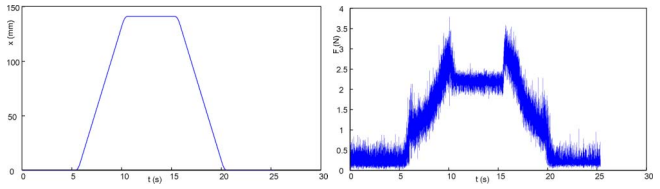

Fig. 11. Endoscope position and friction forces at 30 mm/s.

Typical responses for the endoscope linear velocity, the motor current and the position error over time, are shown in Figs. 12 and 13.

A number of additional experiments were also conducted to investigate the effect of decreasing lubrication, as the endoscope moved in and out of the latex tube repeatedly. It was found that the average force increases by 0.5 N after 5 repetitions of endoscope insertions/ retractions.

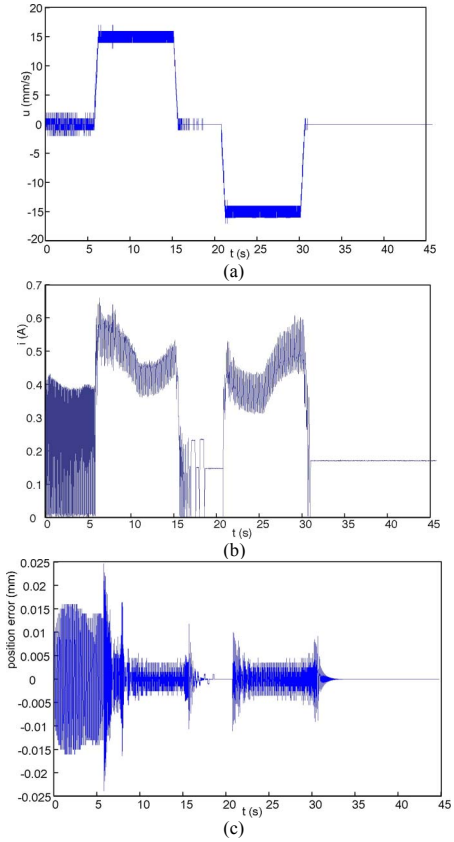

Fig. 13. (a) Endoscope linear velocity, (b) motor current, and (c) position error for 15 mm/s.

V. Model Development

The obtained force results were processed with FFT to identify noise frequencies. A Butterworth filter of 2nd order with elimination frequency at 1/100 of the max was used. After being filtered, the data was truncated to keep the portions at which the endoscope speed was nearly constant. This was true between 30mm to 135mm in the latex tube. The results are shown in Figs. 14 and 15, where the forces developed during the insertion and the retraction phases are shown as a function of endoscope speed.

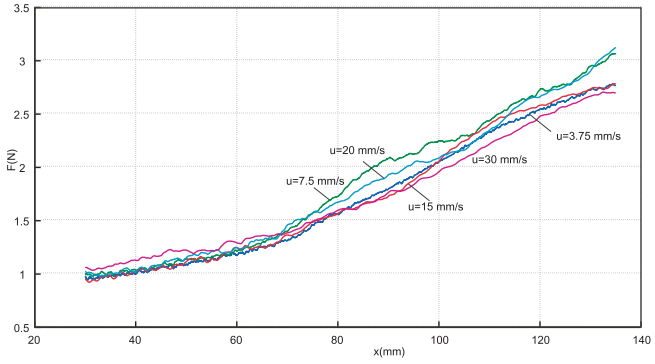

Fig. 14. Endoscope forces during insertion.

These forces were fitted using a least squares approach, using the following approximate force model:

$$F(x,\dot{x}) = F_c + K(x)\cdot x + B(\dot{x})\cdot \dot{x} \qquad (15)$$

where F_c is Coulomb friction, $K(x)$ is the spring constant and $B(\dot{x})$ the corresponding damping. As assumed, the force is function of both the displacement, and the speed.

Two general polynomials of first and second order were used to fit the data:

$$F(x,\dot{x}) = a_0 + a_1 \cdot x + a_2 \cdot \dot{x} \quad (16)$$

$$F(x,\dot{x}) = a_0 + a_1 \cdot x + a_2 \cdot \dot{x} + a_3 \cdot x^2 + a_4 \cdot \dot{x}^2 \quad (17)$$

The following polynomial coefficients were determined for insertion and retraction of the endoscope (all in SI units):

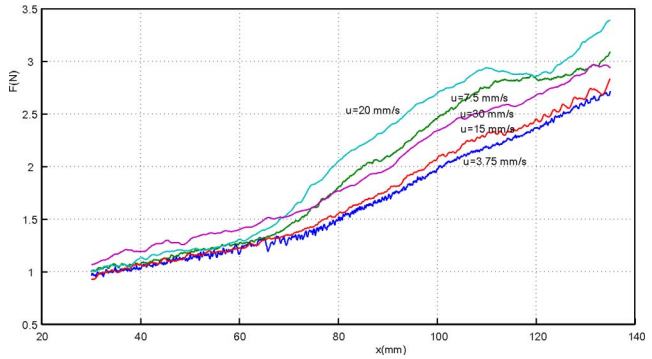

Fig. 15. Endoscope forces during retraction.

1st order model

$$F(x,\dot{x})_{in} = 0.1055 + 0.02 \cdot x + 0.001 \cdot \dot{x} \quad (18)$$

$$K(x) = 0.02 \quad (19)$$

$$B(\dot{x}) = 0.001 \quad (20)$$

Max error: 0.3287

Mean error: 0.0993

$$F(x,\dot{x})_{out} = 0.0732 + 0.0196 \cdot x + 0.0117 \cdot \dot{x} \quad (21)$$

$$K(x) = 0.0196 \quad (22)$$

$$B(\dot{x}) = 0.0117 \quad (23)$$

Max error: 0.4850
Mean error: 0.1518

2nd order model

$$F(x,\dot{x})_{in} = 0.6322 + 0.0036 \cdot x + 0.0147 \cdot \dot{x} + 0.0001 \cdot x^2 - 0.0005 \cdot \dot{x}^2 \quad (24)$$

$$K(x) = (0.0036 + 0.0001 \cdot x) \quad (25)$$

$$B(\dot{x}) = (0.0147 - 0.0005 \cdot \dot{x}) \quad (26)$$

Max error: 0.2568
Mean error: 0.0626

$$F(x,\dot{x})_{ret} = 0.4557 + 0.006 \cdot x + 0.0353 \cdot \dot{x} + 0.0001 \cdot x^2 - 0.0008 \cdot \dot{x}^2 \quad (27)$$

$$K(x) = (0.006 + 0.0001 \cdot x) \quad (28)$$

$$B(\dot{x}) = (0.0353 - 0.0008 \cdot \dot{x}) \quad (29)$$

Max error: 0.4593
Mean error: 0.1248

Comparing the results for the 1st and 2nd order models, we observe that the mean error is of the same order of magnitude. By using the 2nd order model, we can see some small improvement in force approximation. On the other hand, if we need a speedier response in the computation of the model, a 1st order model is more appropriate.

VI. Conclusions

Surgical training simulators are based on the interaction of a haptic interface with the virtual environment. The more realistic this interaction is, the better the training of the young surgeon. A realistic interaction requires a good and accurate model that describes the tissue deformation. In this paper, we deal with the tube shaped tissue deformations that happen during an endoscopic surgery. Such tissues exist in the male urethra surgery and belong to soft tissues. Soft tissues show great non linear material behavior so direct experimental measurements are required. To achieve this we built a device capable of reproducing the endoscopic conditions and measure the developing forces.

The device consists of a mechatronic ball screw mechanism, with a 6 DOF force/ torque sensor attached to it. The steel shaft representing the endoscope is commanded to follow a desired trajectory with micrometric accuracy under the application of an IPD controller implemented on a dSpace 1103 system. The experimental data acquired is fitted to polynomials to yield a tissue model that can be used to predict insertion forces required for haptic simulator feedback. First and second order force models were developed. Although the second order model is more accurate, the first order model computes faster and can be used if computation time is critical.

References

[1] Vlachos K., Papadopoulos, E. and Mitropoulos, D., "Design and Implementation of a Haptic Device for Urological Operations," *IEEE Transactions on Robotics and Automation*, Vol. 19, No. 5, October 2003, pp. 801-809.

[2] Kerdok, A. E., Socrate, S. and Howe, R. D., 2 "Soft tissue modeling and mechanics", *Proc. 28th Amer. Society of Biomechanics Annual Conf.*, poster 235, X-CD Technologies Inc., Portland, OR, 2004.

[3] Kalanovic, D, MP Ottensmeyer, J Gross, G Buess, S. Dawson, "Independent testing of soft tissue viscoelasticity using indentation and rotary shear deformations", *Studies in Health Technology and Informatics*, v. 94, 2003, pp. 137-43.

[4] Brown, JD, J Rosen, YS Kim, L Chang, MN Sinanan, B Hannaford, "In-Vivo and In-Situ Compressive Properties of Porcine Abdominal Soft Tissues", MMVR v. 94, Newport Beach, CA (2003), pp. 26–32.

[5] James T. Hing, Ari D. Brooks and Jaydev P. Desai, "A biplanar fluoroscopic approach for the measurement, modeling, and simulation of needle and soft-tissue interaction", Medical Image Analysis, v. 11, No 1, February 2007, pp. 62-78.

[6] Y.C. Fung, *Biomechanics: Mechanical Properties of Living Tissues*, Springer-Verlag, New York USA, 1993

[7] Abolhassani, JD, R. Patel, M. Moallem, "Needle insertion into soft tissue: A survey", *Medical Eng. & Physics*, v. 29, No. 4, pp. 413-431.

[8] O'Dwyer, Aiden, *Handbook of PI and PID Controller Tuning Rules*, Imperial College Press, London UK, 2003.

[9] Rosenberg R, Karnopp D. *Introduction to Physical System Dynamics*, McGraw Hill, New York NY, 1983.